Digital Discovery

ROYAL SOCIETY OF CHEMISTRY

PAPER

View Article Online
View Journal | View Issue

Cite this: *Digital Discovery*, 2025, **4**, 3810

CatBot – a high-throughput catalyst synthesis and testing system with roll to roll transfer

Paolo Vincenzo Freiesleben de Blasio, * Rune Kruger, Nis Fisker-Bødker, Jin Hyun Chang and Christodoulos Chatzichristodoulou

Received 10th September 2025
Accepted 5th November 2025

DOI: 10.1039/d5dd00403a

rsc.li/digitaldiscovery

Fast and accurate synthesis and testing of electrocatalysts is essential to accelerate development of next generation catalysts for sustainable energy technologies. In this paper, we introduce CatBot, a fully automated platform for reliable synthesis and testing of electrocatalysts capable of operating at temperatures of up to 100 °C from highly acidic to highly alkaline conditions. The platform leverages roll-to-roll transfer, integrating customizable stages for substrate cleaning, catalyst loading, and electrochemical testing, with a custom made liquid distribution system enabling multi-element electrocatalyst synthesis *via* electrodeposition. CatBot enables fabrication and testing of up to 100 electrocatalysts per day, significantly accelerating catalyst discovery and optimization. We demonstrate the platform's reproducibility, through synthesis and testing of various catalytic coatings for the hydrogen evolution reaction (HER) in alkaline conditions, achieving overpotential uncertainties in the range of 4–13 mV at −100 mA cm^{-2}. Additionally, we benchmark the platform by comparing anodic and cathodic redox peaks for nickel in alkaline solutions confirming consistency with previous studies. Thus, CatBot comprises an automated, fast, reproducible, accurate and scalable synthesis and testing system for the accelerated development of next generation electrocatalysts.

1 Introduction

The green transition relies on the deployment of efficient and low-cost electrochemical technologies and catalytic processes that can convert renewable electricity into sustainable fuels and chemicals. Central to this are electrocatalysts that are not only active and stable but also affordable and scalable to industrial levels.[1,2]

However, the discovery and optimization of new electrocatalysts remains time- and resource-intensive, constrained by complex multistep synthesis and characterization processes. When performed manually, researchers are restricted to exploring only a narrow slice of the vast compositional and synthetic parameter space, leaving many promising candidates undiscovered. Furthermore, it is by now well established that electrocatalysts often evolve during operation, their performance depending sensitively on their operating history–yet these effects are rarely studied in depth due to time and resource limitations. Similarly, essential repetitions to assess reproducibility and derive statistical uncertainties are scarcely reported. To combat these limitations, increasing efforts are directed toward lab automation in catalyst research and materials science.[3–6]

Self-driving laboratories (SDLs) offer a solution by automating repetitive tasks and enabling high-throughput experimentation with improved accuracy and repeatability, thereby increasing the reproducibility and statistical reliability.[7] These systems can systematically explore broader regions of the compositional, synthetic, and operational parameter space in a shorter period with adequate repetitions. As such, SDLs have the potential to significantly accelerate the discovery and subsequent optimization of electrocatalysts needed for next-generation energy and chemical conversion systems.

Despite the advancements, many current SDL platforms remain inaccessible due to high hardware cost, proprietary software, and limited modularity. A lack of modularity severely limits adaptation to the evolving research needs and constrains the integration of custom synthesis or characterization steps.[8] Many SDL platforms are often miniaturized, as this reduces running costs and allows for more rapid screening of a large number of samples. While miniaturization offers many benefits, it can amplify the impact of small experimental artifacts.[9] Moreover, scaling up synthesis methods is not always successful and remains a great challenge.[7]

In this work, we present CatBot, a low-cost, high-throughput robotic platform for synthesis and testing of electrocatalytic coatings in both acidic and alkaline media at temperatures of up to 100 °C. The platform utilizes a facile roll-to-roll transfer mechanism that enables fully automated cycling through synthesis and testing steps without the need for robotic arms or human

Technical University of Denmark (DTU), Fysikvej bygning 310, Kongens Lyngby, Denmark. E-mail: ccha@dtu.dk

intervention. CatBot's modular architecture allows for easy integration of additional processing steps such as preconditioning, heat treatment, and in-line characterization. The platform supports reproducible fabrication and testing of up to 100 catalyst-coated samples per day using a user-defined electrodeposition protocol that is easily transferable to larger and more industrial electrode formats. Furthermore, it can accommodate a variety of substrate materials used for the catalytic coating. The reproducibility and robustness of the platform are demonstrated here using both bare nickel and electrodeposited nickel coatings on nickel for alkaline water electrolysis at 80 °C, 6.9 M KOH.

2 Related work

A range of open-source platforms for automating catalyst synthesis and screening has been developed to meet the growing need for high-throughput experimentation. These systems generally fall into two categories: (1) platforms centered around robotic arms that mimic human movements to automate synthesis and testing procedures and (2) systems based on liquid-handling techniques, including automated pipetting and flow controllers.

High-throughput catalyst synthesis is most commonly performed using either inkjet printing[10,11] or automated pipetting combined with drop casting,[6,12,13] both of which can easily generate large batches of catalysts efficiently. These are often coupled with high throughput screening methods such as scanning droplet cells,[14,15] enabling electrochemical measurements to quantify the activity of many samples. However, the key challenge remains: linking activity and stability measurements obtained from such miniaturized, high-throughput systems to technologically relevant electrode architectures. Additionally, scaling the synthesis protocols developed in these small-format setups to industrial applications presents significant difficulties.[7]

Compared to these methods, electrodeposition offers distinct advantages for catalyst synthesis. It enables precise control of the deposition *via* tuning applied current or voltage and produces strong bonding between the catalytic layer and the substrate.[16] Electrodeposition is also already widely employed in catalyst research and technological electrode production at the industrial scale. Despite its relevance, only a limited number of automated, high-throughput platforms leveraging electrodeposition have been developed. Fatehi *et al.*[3] employed a robotic arm in combination with a liquid distribution system to optimize the stability and activity of earth-abundant mixed-metal oxide catalysts for the oxygen evolution reaction (OER). Similarly, Yu *et al.*[17] developed an automated electrodeposition setup that deposited catalysts onto carbon fiber substrates, later removing the catalyst layer *via* electrodissolution for substrate reuse. While these systems represent important progress, they typically operate only under near-ambient conditions and low current densities or rely on costly robotic arms to simulate manual sample handling. Furthermore, expanding such platforms to include additional capabilities, such as pre-treatment or pre/post-conditioning, remains technically challenging due to limited modularity.

3 Experimental setup

CatBot leverages a streamlined roll-to-roll architecture, combined with a liquid distribution system, to automate catalyst synthesis and electrochemical testing (Fig. 1a). At the core of the platform is the roll-to-roll transfer mechanism that moves a continuous substrate through sequential processing stations—including pre-treatment, cleaning, synthesis, and electrochemical testing—without the need for robotic arms or manual intervention. This approach enables continuous operation rather than the traditional batch-based workflows employed in many existing autonomous catalyst platforms.

The roll-to-roll design also introduces a high degree of modularity, allowing individual stations to be reconfigured, expanded, or swapped out to meet the demands of evolving workflows. After synthesis and testing, the coated catalyst samples are collected on a take-up drum, enabling storage for subsequent post-mortem characterization.

The CatBot was designed to meet the following key design requirements:

1. The system must operate reliably in harsh electrochemical environments, including highly alkaline (>30 wt% KOH) and acidic (3 M HCl) media, at temperatures up to 100 °C to evaluate catalyst activity/stability in realistic environments.

2. Each processing stage (*e.g.*, pre-treatment, electrodeposition, post-treatment, testing) should be easily interchangeable or extendable to accommodate different (electro)catalytic applications or characterization needs.

3. The system must support electrodeposition as the primary synthesis method due to its industrial relevance, versatility, and ability to generate strongly adhered, compositionally tunable catalyst layers.

4. Sample holders and reagent volumes should balance measurement precision with efficient use of chemicals and materials, minimizing waste while maintaining data quality.

3.1 Roll-to-roll system

The roll-to-roll system automates substrate transfer through sequential stages of cleaning, synthesis, and electrochemical testing. A spool of substrate (*e.g.*, Ni wire) is mounted at the inlet (left side of Fig. 1a and b), and a stepper motor connected to a custom 3D-printed take-up drum on the opposite end regulates its movement through the system (Fig. S1). The substrate first passes through two cleaning stations. In the first, it is immersed in a 3 M HCl to remove oxides and surface contaminants. It then enters a water rinse station to eliminate residual acid, ensuring a clean surface for subsequent catalyst coating. The substrate then enters the synthesis station, where electrodeposition takes place to form an electrocatalytic coating. A metal salt electrolyte is used, and a potential is applied between the substrate and a counter electrode to drive the deposition process.

After coating, the electrode is transferred directly to the testing station, where its electrochemical performance is evaluated. In this work, the platform is demonstrated using the hydrogen evolution reaction (HER), though it is compatible

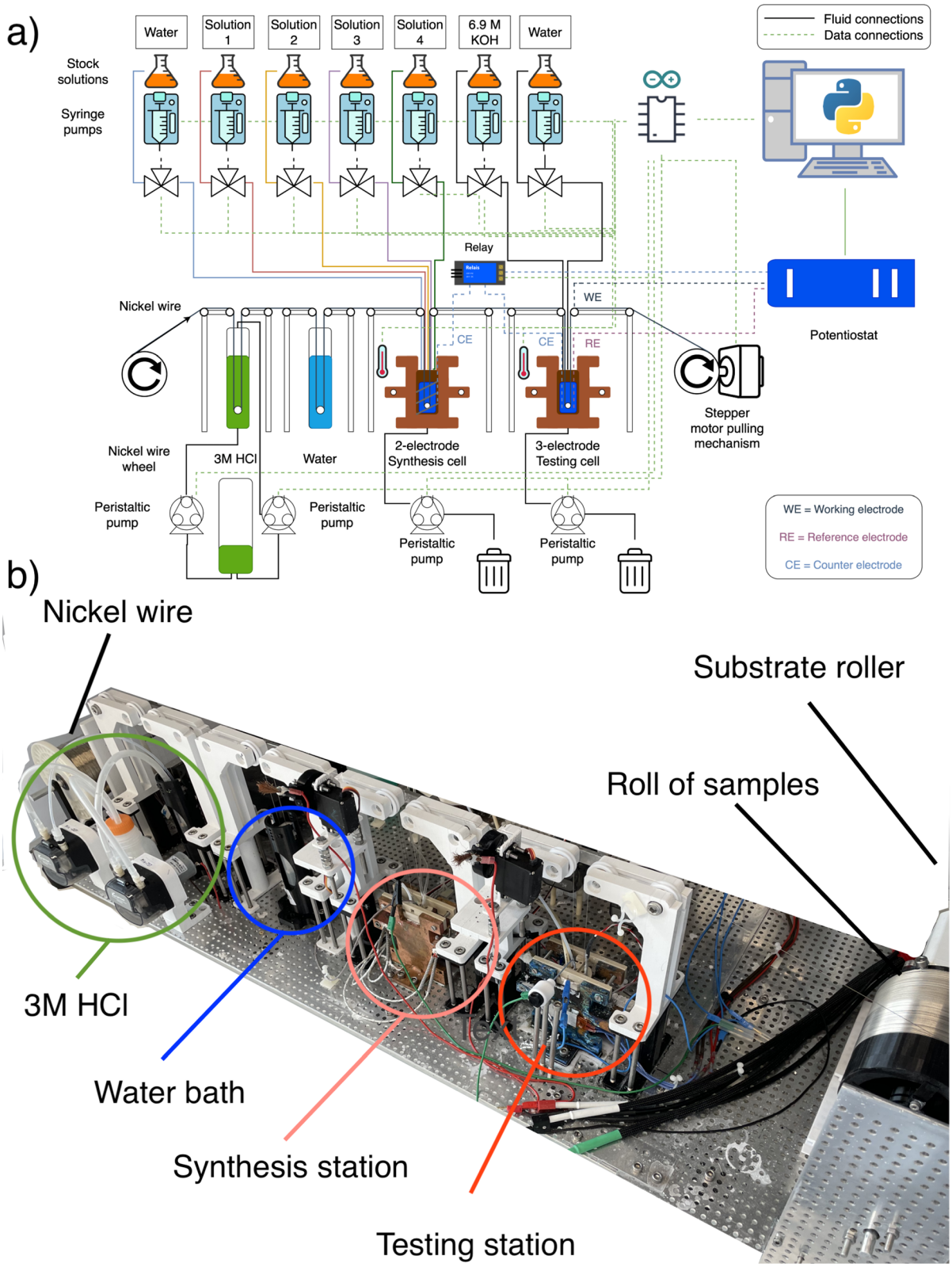

Fig. 1 Overview of the CatBot roll-to-roll catalyst synthesis and testing platform. (a) Schematic of the full system layout, showing components and fluid and data connections. (b) Zoom-in on the roll-to-roll substrate transport system (bottom portion of the schematic), highlighting the stations the substrate (nickel wire) passes through during synthesis and testing.

with a broad range of electrocatalytic applications, including oxygen evolution reaction (OER), CO_2 reduction reaction (CO_2RR), and corrosion protection. Following testing, the coated substrate is rolled onto the take-up drum, allowing for sample retrieval and characterization. The system then returns to its starting state and proceeds with the next experimental segment. The electrical connection between the potentiostat and substrate is maintained using a metal brush mounted on a servo motor, which rotates to ensure stable contact during operation (Fig. S2).

As the system includes two stations requiring potentiostat control, a relay is used to switch between configurations: a two-electrode setup in the synthesis station and a three-electrode setup in the testing station, enabling the use of a single potentiostat for both chambers.

3.2 Liquid distribution system

The liquid-handling system comprises seven syringe pumps that enable precise delivery of liquids to the synthesis and testing stations, with a resolution of 30 μL. In the current configuration, five syringe pumps are assigned to the synthesis station and two to the testing station. The system is designed for scalability and modularity, allowing pumps to be redistributed or added as experimental needs evolve.

Each syringe pump is driven by a stepper motor controlled through a motor driver connected to an Arduino microcontroller. The syringe pumps are coupled with three-way valves actuated by servo motors, also operated by the Arduino (Fig. S4). This configuration allows the system to switch automatically between aspiration and dispensing modes, enabling self-refilling when the syringes reach low volumes.

Waste management is handled by peristaltic pumps connected to the drainage outlets at the bottom of the synthesis and testing stations. These pumps remove spent liquids following experiments or cleaning cycles and direct them into a waste container (Fig. 2).

All components in contact with liquids, including syringes, tubing, and reagent bottles, are made of polypropylene (PP), selected for its high chemical resistance and stability. This ensures compatibility with a broad range of electrolytes and prevents contamination or material degradation over time.

During operation, the synthesis and testing chambers are filled with 15 mL and 11 mL of liquid, respectively. A volumetric variation of 30 μL corresponds to an uncertainty of approximately 0.2% to 0.27%, depending on the chamber, which is considered adequate. Further improvement in dispensing precision can be achieved by using tubing with a smaller internal diameter, thereby reducing droplet size, which remains the key contributor to the indicated uncertainty.

In the example described in this work, two syringe pumps were connected to the synthesis station: one containing a 0.4 M $NiSO_4$ and 0.4 M $Na_3C_6H_5O_7$ (sodium citrate) precursor solution, and the other containing Milli-Q water. Combining $NiSO_4$ and Milli-Q water allows the concentration to be adjusted. The Milli-Q water supply is also used to clean the synthesis chamber between runs. The two syringe pumps connected to the testing station contained Milli-Q water and 6.9 M KOH. The water served dual roles, diluting the KOH as desired and rinsing the testing chamber during cleaning cycles.

3.3 Chamber design

The synthesis and testing chambers, which hold the electrolyte solutions, were CNC-milled from polyether ether ketone (PEEK). PEEK was selected for its excellent mechanical properties and chemical stability in alkaline and acidic environments at elevated temperatures. The synthesis chamber consists of two main components: a main container and a removable lid. The lid features a PEEK holder for a Ø7 mm bearing made of PEEK and zirconia, which guides the moving substrate through the chamber. Two PEEK rods mounted on the lid hold a Pt wire that serves as the counter electrode (Fig. S5).

The testing chamber follows a similar design. The lid includes a Ø7 mm PEEK bearing holder for substrate guidance, while the main container houses a removable insert that holds both the membrane/diaphragm and the perforated nickel plate counter electrode (CE), as shown in Fig. 2, element 10. This holder, 3D-printed in PEEK, is positioned close to the coated Ni wire working electrode (WE). The internal geometries of both chambers are modular and can be easily reconfigured to accommodate other experimental requirements.

Fig. 2a presents a cross-sectional view of the testing station. The nickel wire substrate enters the chamber from the top and is rolled through the Ø7 mm bearing at the bottom. Two copper brackets securely fix the chambers during experimentation, and allow for an even distribution of the heat from the heating cartridges that are fixed on them. A temperature probe is submerged into the liquid electrolyte and another one in the copper bracket itself. This allows for a fast and accurate temperature control. The reference electrode is placed between the nickel wire substrate and the perforated nickel plate counter electrode. In this study, a Zirfon separator was placed between the reference electrode and the counter electrode to prevent hydrogen and oxygen bubbles from mixing during testing.

3.4 Electronics and software

Control of all electronic components of the setup including syringe pumps, peristaltic pumps, servo motors, and heating elements is facilitated through Arduino. Two Arduino MEGAs are employed in the platform. The first Arduino controls the roll-to-roll and liquid handling systems, while the second monitors and sets the temperature of the synthesis and testing stations. The Arduinos are placed on custom made printed circuit boards (PCBs) to reduce wiring complexity and simplify repairs. To programmatically control and monitor the electronic components of the setup, serial communication between Python and the Arduinos is established through the pyserial package.

The workflow is managed by the catbot_control_master.py script, which interfaces user-control of all electronic components in the setup. This script calls on several subpackages in Python, that in turn communicate directly with Arduino, to control key functionalities of the platform such as substrate

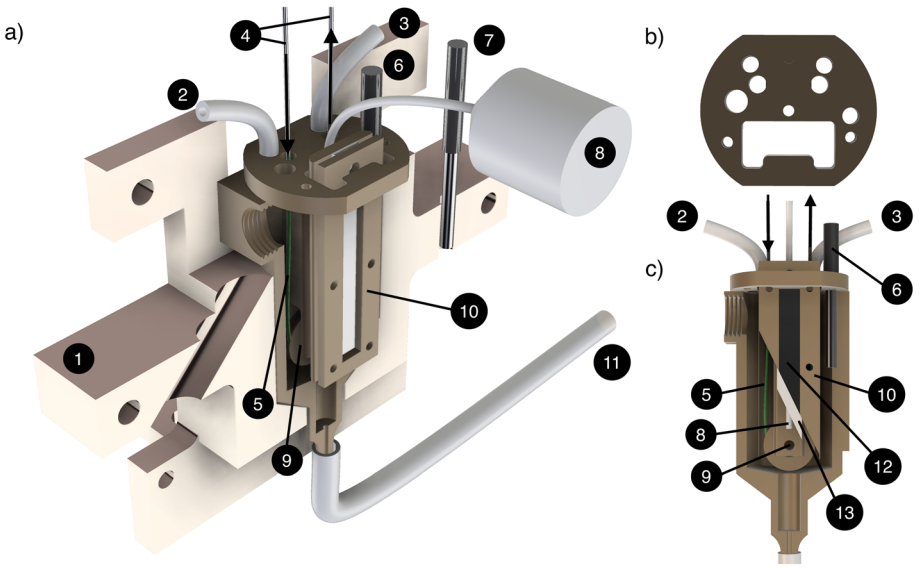

Fig. 2 (a) Sectional 3D render of the PEEK testing chamber placed inside with (1) heating copper bracket, which is connected to heating elements (not shown), (2) water inlet, (3) KOH inlet, (4) uncoated nickel wire, [WE], (5) applied catalytic coating (6) temperature probe monitoring the electrolyte temperature (7) temperature probe for copper bracket, (8) RHE reference electrode, (9) bearing composed of PEEK and zirconia (10) CE and separator holder (11) tubing that goes to peristaltic drain pump and further to waste (12) nickel perforated plate CE, (13) Zirfon 500 separator. (b) Top view of the lid with designated openings for the nickel wire, counter electrode, reference electrode, temperature probe and electrolyte inlets. (c) Sectional side view of the PEEK testing chamber with the lid.

transfer, waste handling, liquid distribution and temperature settings. To execute an experiment, the user defines the key parameters, such as synthesis conditions, testing conditions, testing protocol and cleaning protocol. An example script for running an experiment, showing the possible parameter selections is presented in (Listing S.1). Additional functionalities can easily be implemented, as all instruments can be controlled from high-level Python code. Finally, the Squidstat potentiostat is controlled directly from Python using their custom made API. To simplify integration into our software package, we wrote a wrapper around their API.

4 Electrochemical reproducibility of the platform

4.1 Reproducibility and consistency in oxidation and reduction peaks of nickel

Ni has a well-defined oxidation peak at approx. ~1.4 V *vs.* RHE in alkaline conditions, where α/β-$Ni(OH)_2$ oxidizes to β-NiOOH.[18–23] To ensure accuracy and reproducibility of the platform, we investigated the peak location when cycling 8 uncoated Ni wires at two different conditions: 4 wires cycled at T = 80 °C in a 6.9 M KOH solution and 4 wires cycled at T = 30 °C in a 0.5 M KOH solution. Fig. 3a and b show the second and tenth CV curves for the wires cycled at the two different conditions. When cycling at T = 30 °C, the initial location of the oxidation peak is at 1411.2 mV with an uncertainty of ±1.3 mV. Increasing the temperature and concentration of KOH shifts the anodic and cathodic peaks to lower values, with the anodic peak now at 1372.7 mV ± 1.4 mV. Moreover, the intensity of the anodic peak increases significantly. In the tenth cycle (Fig. 3b), the location of the peak remains nearly unchanged at 1407.2 mV ± 3.8 mV when cycling at T = 30 °C, 0.5 M KOH, whereas it shifts slightly to 1379.1 mV ± 0.5 mV at T = 80 °C, 6.9 M KOH. Compared to cycling at 30 °C, we observe the growth of a peak at roughly 1500 mV at 80 °C. While the origin of this peak is not well-established, it could be related to the growth of an energetic γ phase NiOOH.[18] The results are in good agreement with previously reported peak positions, finding the α/β-$Ni(OH)_2$ to β-NiOOH transition lying at 1360–1370 mV *vs.* RHE in 1–6 M KOH Fe-free solution at T = 25 °C, shifting towards 1380–1420 mV *vs.* RHE with trace levels of Fe impurities, and to even higher potentials with increasing Fe content in the electrolyte.[20,21] This suggest that trace levels of Fe are present in our KOH, which is expected given that we only perform pre-electrolysis and no further purification with $Ni(OH)_2$. The measurement uncertainty of the peak positions was below 5 mV at all experimental conditions. The experiments conducted in the platform are therefore highly reproducible while spanning a broad range of electrolyte concentrations and operating temperatures.

4.2 ECSA

The ECSA was estimated from the double-layer capacitance (C_{dl}), determined from the slope of the current density *versus* scan rate in the non-faradaic region, using the relationship ECSA = C_{dl}/20 μF cm^{-2}, where 20 μF cm^{-2} was taken to represent the C_{dl} value of the perfectly smooth electrode.[24] Calculated ECSA values, along with their corresponding standard deviations, are presented in Table 1. The bare Ni wire exhibits the lowest ECSA at 4.3 cm^2 ± 0.2 cm^2 demonstrating consistency for the smooth Ni surface. As a coating is applied onto the

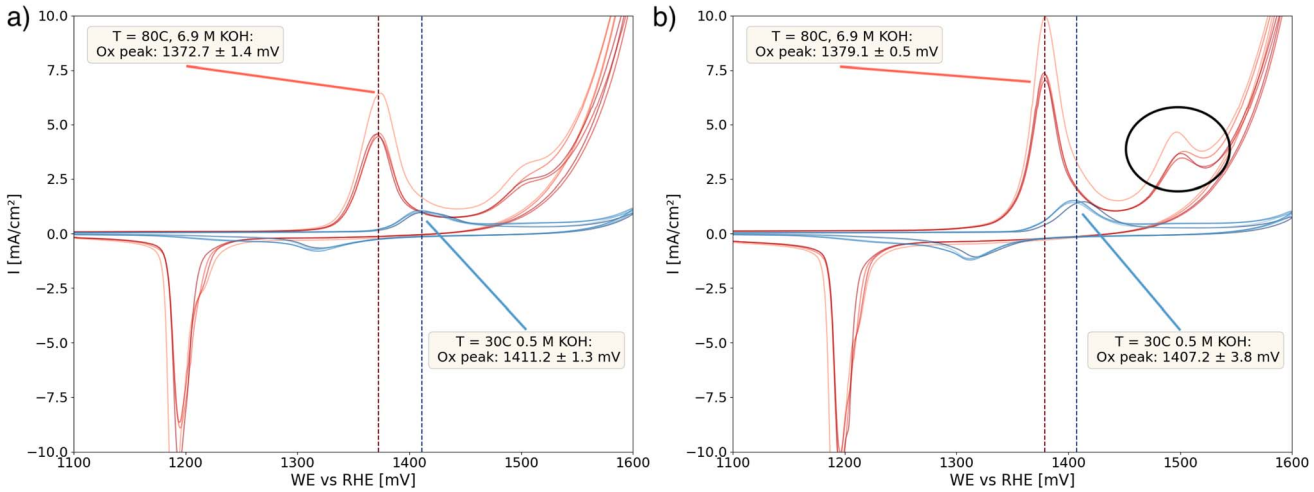

Fig. 3 Comparison of the voltammograms between the 4 uncoated wires cycled at 6.9 M KOH at 80 °C (red curves), and 0.5 M KOH at 30 °C at 50 mV s^{-1} (blue curves) (a) overlaid voltammograms of the 2nd CV cycle of the Ni wires cycled at different conditions with peak positions marked. (b) Overlaid voltammograms of the 10th CV cycle of the Ni wires cycled at different conditions with peak positions marked.

Table 1 Determined ECSA values and their corresponding standard deviations for bare nickel wire and coated electrodes

	ECSA [cm^2]	Uncertainty [cm^2]	Error [%]
Bare wire	4.3	0.2	4.7%
S1	197.5	28.7	14.5%
S2	45.6	9.4	20.6%
S3	619.8	36.3	5.8%

electrode, the ECSA increases by a factor of 10–150. Even when applying a coating, the uncertainties in ECSA range from 4.7% to 20.6% remaining within an acceptable range.

4.3 HER activity of bare and coated wires

We then investigated the HER activities of the coated and uncoated samples. Fig. 4a) reports the LSVs obtained from 0 mV to −500 mV recorded at 5 mV s^{-1} in 6.9 M KOH at 80 °C. The current density was capped at −100 mA cm^{-2}, to avoid excessive foaming of the electrolyte at higher current densities. The bare Ni wire exhibited the highest overpotential at −10 mA cm^{-2} η_{10} = 421 mV. A higher ECSA correlated with lower η_{10} and η_{100} values. The sample-to-sample reproducibility of these experiments is remarkable. The overpotential values for the bare and coated wires span η_{10} = 220–421 mV and η_{100} = 335–451 mV with standard deviations in the range 4.2–13 mV (Fig. 4b). These results demonstrate the platform's suitability for both fundamental mechanistic studies and high-throughput screening of electrocatalyst coatings.

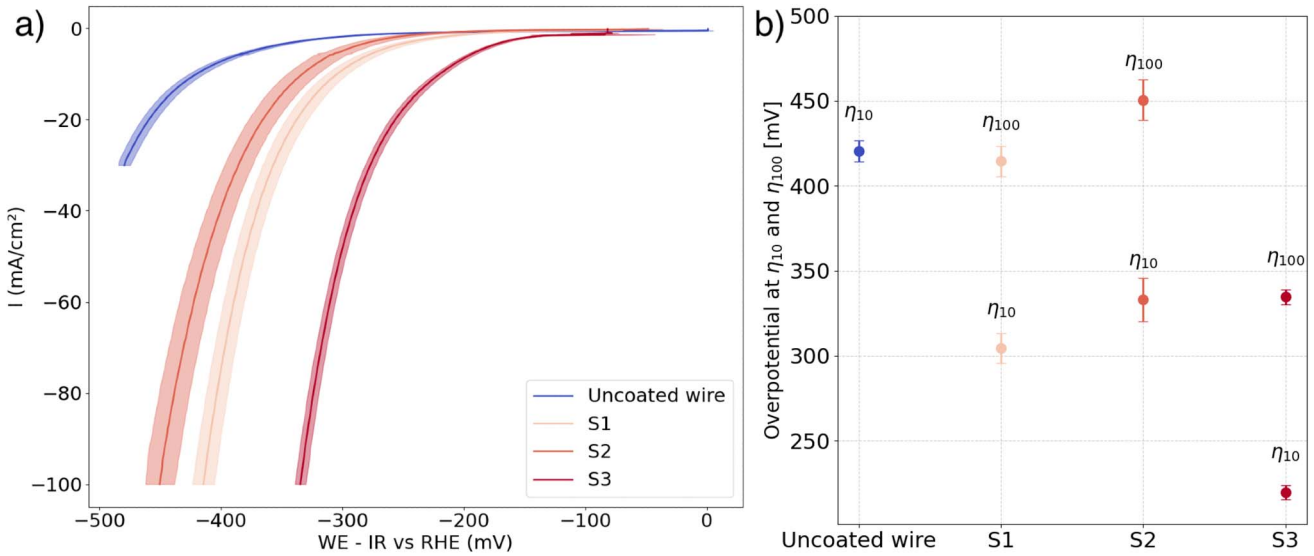

Fig. 4 HER catalytic performance evaluation (a) LSVs in 6.9 M KOH at 80 °C at 5 mV s^{-1} IR corrected. (b) Mean overpotentials at η_{10} (CC 10 mA cm^{-2}) and η_{100} (CC 100 mA cm^{-2}).

Table 2 Deposition parameters for nickel coatings

	$NiSO_4$ [M]	Time [s]	I [mA cm^{-2}]	Temp. [°C]
S1	0.15	120	150	45
S2	0.1	150	80	55
S3	0.1	250	200	60

5 Conclusion

In this work we introduce CatBot (Catalysis Bot), a fully automated platform capable of synthesizing and testing electrocatalysts. The platform was designed to be low cost, chemically resistant to concentrated acids and bases at higher temperatures, as well as modular, allowing easy integration of additional functionalities such as additional pre-treatment or heat treatment steps. It utilizes a novel roll-to-roll system for both fabrication and testing of electrocatalysts without any moving parts or robotic arms, improving both reliability and safety. The platform was benchmarked by investigating characteristic oxidation and reduction peaks of Ni, showing both a high degree of reproducibility and consistency with previous studies. Moreover, different coatings were applied to a Ni wire in order to evaluate the consistency of catalytic coating application and testing. This yielded uncertainties of HER overpotentials on the order of 4 mV to 12 mV for different coatings at −10 to −100 mA cm^{-2}, corresponding to a maximum uncertainty of 3%. Simultaneously, the platform is both durable and efficient, managing to perform all 20 experiments described here in just 20 hours. In the present configuration, catalytic coatings are deposited onto a substrate *via* electrodeposition. Nonetheless, modifications can effortlessly incorporate alternative synthesis techniques such as electroless plating, dip-coating, spraying, and more if needed.

The next step is to integrate machine learning (ML) with the platform for autonomous synthesis, testing, and optimization of catalytic coatings. ML is becoming prominent in catalysis by identifying complex parameter trends, resulting in accelerated catalyst discovery and generation of fundamental insights.[3,6,25] We believe that our system and other SDLs, when integrated with machine learning algorithms, will significantly accelerate the discovery of highly stable and active catalysts. Moreover, it is important to highlight that the platform we have introduced is versatile enough to be applied in numerous applications. While illustrated here for the optimization of electrocatalysts, it can also be tailored for a wide range of areas, including corrosion science and bioelectrochemical sensing.

6 Chemicals and materials

6.1 Chemicals and materials

37 wt% HCl with a purity of 99.999% was purchased from Sigma-Aldrich, and subsequently diluted down to 3 M using Milli-Q water. Nickel sulphate hexahydrate with a purity of 98.5% and sodium citrate dihydrate with a purity of 99% were also acquired from Sigma Aldrich. KOH pellets were obtained from VWR chemicals and aqueous KOH electrolyte was prepared at a concentration of 30 wt% and then pre-electrolysed for 72 hours to remove metal impurities present in the KOH pellets. A 1 km roll of Ø0.4 mm nickel wire with a purity of 99.8% was purchased from Changzhou dlx alloy Co.

6.2 Electrochemical measurements

All electrochemical measurements were performed using an Admiral Squidstat Plus potentiostat. The electrodeposition took place in a two electrode chamber with the Ni wire as WE, and a spooled Ø0.4 mm Pt wire acting as the CE. The potential used in the plating was WE *vs.* CE. The electrochemical testing was performed in a three electrode testing chamber with a Ni perforated plate as CE, and a Ø1.6 mm Gaskatel Mini Hydroflex reversible hydrogen electrode (RHE) as reference electrode (RE).

6.3 Experimental protocol

To assess platform accuracy and reproducibility, we conducted a qualification and benchmarking study focusing on the consistency and accuracy of the electrochemical data obtained from both bare and coated Ni wires. Ni wire was selected due to its low cost and well defined geometric surface area. During the experiments, only one sample was processed at a time. The Ni wire underwent cleaning in 3 M HCl for 15 minutes prior to any experimentation. The HCl was emptied into a separatecontainer after the cleaning procedure. Uncoated Ni wire was tested in 6.9 M KOH at 80 °C and 0.5 M KOH at 30 °C to assess anodic and cathodic Ni redox peak position reproducibility. Peak positions were also compared with literature to assess consistency. Moreover, the uncoated Ni wire tested at 80 °C served as a baseline to compare the catalytic activity of the coated Ni samples. Each experiment was repeated 4 times for both coated and uncoated Ni. A citrate bath containing 0.4 M $NiSO_4$ and 0.4 M trisodium citrate, and adjusted to a pH of 2 using concentrated sulfuric acid, was used for the electrodeposition baths. For different coatings, the Ni precursor solution was diluted with Milli-Q water, while maintaining the $NiSO_4$-to-citrate ratio. To validate the platform's sample-to-sample reproducibility over a broad range of deposition conditions, three different sets of coating parameters were chosen, listed in Table 2. Uniform coating on the Ni wire was achieved by continuously moving the Ni wire during the electrodeposition process as illustrated in Fig. S7.

Following cleaning in 3 M HCl and water, and electrodeposition for the coated Ni wire, a multi-step electrochemical protocol was employed. The protocol begins with a galvanostatic electrochemical impedance spectroscopy (GEIS) measurement at a current density of −10 mA cm^{-2} from 100 kHz to 1 Hz to obtain the solution resistance (R_s). This is followed by CV scans in the non-faradaic region 50–150 mV *vs.* RHE at scan rates of 20, 40, 80, 160, and 320 mV s^{-1} to determine the electrochemical surface area (ECSA). LSV is then performed from 0 to −500 mV *vs.* RHE at 5 mV s^{-1} to evaluate HER activity at different overpotentials. Finally, the bare wires undergo 10 CV cycles from −200 mV to 1600 mV *vs.* RHE at 50 mV s^{-1}, to assess consistency and reproducibility of the

redox peaks of the bare Ni surface. The coated wires followed the same protocol, where the last 10 CV cycles were omitted as we were only interested in the reproducibility of the ECSA of the applied coating, and the overpotentials at -10 mA cm^{-2} and -100 mA cm^{-2}. After each experiment, both the deposition and testing electrolytes were flushed, and the corresponding chambers were rinsed twice with Milli-Q water following deposition and testing, respectively. The total experimental time for coated electrodes was 40–50 minutes, including HCl cleaning, deposition, and electrochemical testing. For bare nickel wire, each experiment took 40–45 minutes, including HCl cleaning and electrochemical testing.

Author contributions

P. V. F. D. B.: conceptualization, methodology, investigation, data analysis, software, visualization, writing – original draft R. K.: methodology, investigation, software, writing – review and editing N. F. B.: methodology, writing – review and editing, J. H. C.: project administration, resources, writing – review and editing, C. C.: conceptualization, resources, project administration, writing – review and editing.

Conflicts of interest

Paolo Vincenzo Freiesleben de Blasio, Nis Fisker Bødker, Jin Hyun Chang and Christodoulos Chatzichristodoulou have a patent pending for a modular roll-to-roll system and method for synthesis, fabrication, characterization, and testing of catalysts and catalytic coatings. Rune Kruger has no conflicts of interest to declare.

Data availability

The code used to run the experiments and control the robotic system is available on GitHub: **https://github.com/Pele905/CatBot_public**. All supporting materials, including 3D models, datasets, and KiCad schematics, are available at Zenodo: **https://doi.org/10.5281/zenodo.15169175**.

Supplementary information is available. See DOI: **https://doi.org/10.1039/d5dd00403a**.

Acknowledgements

The authors acknowledge financial support from the Clean Hydrogen Partnership and its members under the grant agreement SUSTAINCELL (Project No. 101101479). Co-funded by the European Union. Views and opinions expressed are however those of the author(s) only and do not necessarily reflect those of the European Union or the Clean Hydrogen Partnership. Neither the European Union nor the granting authority can be held responsible for them.

Notes and references

1 X. Gao, Y. Chen, Y. Wang, L. Zhao, X. Zhao, J. Du, H. Wu and A. Chen, *Nano-Micro Lett.*, 2024, **16**, 237.
2 J. Liu, J. Ma, Z. Zhang, Y. Qin, Y.-J. Wang, Y. Wang, R. Tan, X. Duan, T. Z. Tian, C. H. Zhang, *et al.*, *J. Phys.: Mater.*, 2021, **4**, 022004.
3 E. Fatehi, M. Thadani, G. Birsan and R. W. Black, *arXiv*, 2023, preprint, arXiv:2305.12541, DOI: **10.48550/arXiv.2305.12541**.
4 J.-M. Lu, J.-Z. Pan, Y.-M. Mo and Q. Fang, *Artif. Intell. Chem.*, 2024, 100057.
5 B. Burger, P. M. Maffettone, V. V. Gusev, C. M. Aitchison, Y. Bai, X. Wang, X. Li, B. M. Alston, B. Li, R. Clowes, *et al.*, *Nature*, 2020, **583**, 237–241.
6 K. J. Jenewein, L. Torresi, N. Haghmoradi, A. Kormányos, P. Friederich and S. Cherevko, *J. Mater. Chem. A*, 2024, **12**, 3072–3083.
7 A. Trunschke, *Catal. Sci. Technol.*, 2022, **12**, 3650–3669.
8 R. Pollice, G. dos Passos Gomes, M. Aldeghi, R. J. Hickman, M. Krenn, C. Lavigne, M. Lindner-D'Addario, A. Nigam, C. T. Ser, Z. Yao, *et al.*, *Acc. Chem. Res.*, 2021, **54**, 849–860.
9 J. Abed, Y. Bai, D. Persaud, J. Kim, J. Witt, J. Hattrick-Simpers and E. H. Sargent, *Digital Discovery*, 2024, **3**, 2265–2274.
10 X. Liu, Y. Shen, R. Yang, S. Zou, X. Ji, L. Shi, Y. Zhang, D. Liu, L. Xiao, X. Zheng, *et al.*, *Nano Lett.*, 2012, **12**, 5733–5739.
11 J. A. Haber, Y. Cai, S. Jung, C. Xiang, S. Mitrovic, J. Jin, A. T. Bell and J. M. Gregoire, *Energy Environ. Sci.*, 2014, **7**, 682–688.
12 K. J. Jenewein, G. D. Akkoc, A. Kormányos and S. Cherevko, *Chem Catal.*, 2022, **2**, 2778–2794.
13 J. M. Przybysz, K. J. Jenewein, M. Minichová, T. Hrbek, T. Bohm, T. Priamushko and S. Cherevko, *ACS Mater. Lett.*, 2024, **6**, 5103–5111.
14 A. K. Schuppert, A. A. Topalov, I. Katsounaros, S. O. Klemm and K. J. Mayrhofer, *J. Electrochem. Soc.*, 2012, **159**, F670.
15 J. M. Gregoire, C. Xiang, X. Liu, M. Marcin and J. Jin, *Rev. Sci. Instrum.*, 2013, **84**(2), 024102.
16 M. B. Lopez and J. Ustarroz, *Curr. Opin. Electrochem.*, 2021, **27**, 100688.
17 C. Yu, Q. Xiong, K. Yang, H. Chen and F. Pan, *Adv. Mater. Technol.*, 2021, **6**, 2001036.
18 M. Alsabet, M. Grdeń and G. Jerkiewicz, *Electrocatalysis*, 2015, **6**, 60–71.
19 D. S. Hall, C. Bock and B. R. MacDougall, *J. Electrochem. Soc.*, 2013, **160**, F235.
20 F. L. Buchauer, A. Russo, E. R. Moretti, S. Iqbal, M. R. Kraglund and C. Chatzichristodoulou, *Electrochim. Acta*, 2024, **500**, 144719.
21 D. A. Corrigan, *J. Electrochem. Soc.*, 1987, **134**, 377.
22 L. Trotochaud, S. L. Young, J. K. Ranney and S. W. Boettcher, *J. Am. Chem. Soc.*, 2014, **136**, 6744–6753.
23 S. Iqbal, J. C. Ehlers, I. Hussain, K. Zhang and C. Chatzichristodoulou, *Chem. Eng. J.*, 2024, 156219.
24 E. Navarro-Flores, Z. Chong and S. Omanovic, *J. Mol. Catal. A: Chem.*, 2005, **226**, 179–197.
25 W. J. Kort-Kamp, M. Ferrandon, X. Wang, J. H. Park, R. K. Malla, T. Ahmed, E. F. Holby, D. J. Myers and P. Zelenay, *J. Power Sources*, 2023, **559**, 232583.